Article | Received 24 June 2026; Revised 21 August 2026; Accepted 25 August 2026; Published date
https://doi.org/10.55092/bm20260007

Immunomodulatory effect of OCP doped with strontium, magnesium, and barium cations *in vitro*

Vladislav V. Minaichev[1,*], Anastasia Yu. Teterina[2], Margarita I. Kobyakova[1], Roman S. Fadeev[1], Igor V. Smirnov[2], Polina V. Mikheeva[2], Mikhail A. Shlykov[2], Kirill A. Agibalov[1], Irina S. Fadeeva[1] and Vladimir S. Komlev[2,*]

[1] Institute of Theoretical and Experimental Biophysics, Russian Academy of Sciences, Pushchino, Russian Federation

[2] Baikov Institute of Metallurgy and Materials Science, Russian Academy of Sciences, Moscow, Russian Federation

* Correspondence authors; E-mails: vminaychev@gmail.com (V.V.M.); komlev@mail.ru (V.S.K.).

Highlights:

- Low-temperature synthesis of Sr/Mg and Sr/Ba co-doped octacalcium phosphate.
- Doped OCP is non-cytotoxic and modulates phagocytosis, ROS, and cytokines.
- Immunomodulation is mediated by particle-cell interaction, not soluble ions.

Abstract: The development of modern osteoplastic materials with controlled immunomodulatory properties represents a critical objective in bone tissue engineering. Octacalcium phosphate (OCP) serves as a promising precursor to bone apatite; however, its clinical application is limited by inconsistent biological response for recipients with similar nosology. Ionic doping presents a prospective approach for enhancing the functional characteristics of calcium phosphates. This study is dedicated to the synthesis and *in vitro* investigation of the immunomodulatory effects of low-temperature OCP co-doped with Sr^{2+}/Mg^{2+} and Sr^{2+}/Ba^{2+}. The developed materials were characterized using X-ray diffraction (XRD) and Fourier-transform infrared spectroscopy (FTIR). The incorporation of strontium during OCP synthesis was shown to destabilize the crystal lattice and reduce crystallite size. *In vitro* studies utilizing monocyte-like (THP-1 ATRA) and macrophage-like (THP-1 PMA) cell models demonstrated that the doped OCP materials did not induce cytotoxic effects and effectively modulated the functional activity of immune cells. Specifically, in monocyte-like cells, both OCP materials enhanced phagocytic activity and significantly increased the secretion of pro-inflammatory cytokines (TNF-α, IL-1β, IL-6). In macrophage-like cells, the materials reduced phagocytic activity and exerted dual ion-dependent effects on reactive oxygen species (ROS) production. Furthermore, they stimulated cytokine secretion predominantly under non-inflammatory conditions. Notably, OCP_Sr20_Mg1 induced a comparatively milder proinflammatory response compared to OCP_Sr20_Ba1, specifically reducing ROS formation and cytokine secretion by monocyte-like and macrophage-like cells under standard conditions. These results suggest that Sr/Mg co-doping may provide a more balanced

immunomodulatory profile favorable for osteoplastic applications. The findings indicate that the immunomodulatory effect is likely mediated through direct particle-cell interactions influencing intracellular processes such as phagocytosis and lysosomal activity, rather than being solely attributable to soluble ion release.

Keywords: octacalcium phosphate; ion doping; strontium; magnesium; barium; immunomodulation; monocytes; macrophages; cytokines; bone tissue engineering

1. Introduction

The creation of highly effective biomaterials for bone regeneration remains a paramount unresolved challenge in contemporary tissue engineering, which is of significant social and medical relevance. This challenge is becoming increasingly relevant in the context of global population aging, which leads to a substantial increase in musculoskeletal disorders such as osteoporosis, osteoarthritis, and other pathologies [1,2]. Concurrently, there is a consistent rise in trauma of various origins, including road accidents, occupational injuries, sports-related damage, and domestic accidents. A distinct and serious medical concern is unforeseen injuries from emergencies, natural disasters, or accidental falls, often leading to complex fractures and extensive bone defects that necessitate the application of osteoplastic materials [3].

Thus, the combined impact of demographic aging and increasing trauma rates generates a sustained demand for novel biomaterials that combine high osteogenic activity with applicability across diverse clinical scenarios [1,4]. This establishes the priority of research focused on developing new generations of osteoplastic materials for regenerative medicine.

Traditional methods for bone defect repair, such as autotransplantation, are often not feasible due to limited availability of graft material and additional trauma to the patient's body, while allogeneic bone tissue usage carries risks of immune rejection and challenges associated with procurement and storage [5,6]. Consequently, synthetic calcium phosphate compounds (CPCs) have gained widespread clinical adoption due to their compositional similarity to bone hydroxyapatite and capacity to stimulate tissue regeneration [7]. However, CPC application is complicated by several factors, including the material's physicochemical parameters, site-specific bone structure, comorbidities, and the patient's immune status [8].

It is well established that the physicochemical parameters of CPCs and their synthesis methods substantially determine their biological properties. Conventional high-temperature synthesis ($t > 1000$ °C) yields chemically stable yet biologically inert materials. Despite their non-toxic nature, the low solubility and coarse crystalline structure of these materials limit their regenerative efficacy, often resulting in fibrous encapsulation as the primary host response [9]. Therefore, utilizing physiological temperatures during synthesis represents a promising approach to enhance the osteogenic properties of CPCs [10]. Materials synthesized through such methods are anticipated to closely resemble the natural bone mineral in structure and, consequently, possess the necessary biological properties for regeneration [11].

In recent years, research interest has increasingly shifted toward investigating the immunomodulatory properties of calcium phosphate materials. The initial interaction between an implant and innate immune cells, particularly monocytes and macrophages, constitutes a critical phase determining the implant's fate. Their polarization into pro- or anti-inflammatory phenotypes directly influences bone regeneration or, conversely, leads to fibrous encapsulation and rejection [12]. However, the relationships

between the physicochemical properties of calcium phosphate compounds (composition, charge, particle size, *etc.*) and immune responses are only beginning to be elucidated [13,14].

Among the broad spectrum of calcium phosphate compounds, octacalcium phosphate (OCP) is of particular interest due to its osteoinductive properties and unique capacity to transform *in vivo* into bone hydroxyapatite and [15]. Nevertheless, OCP application faces several significant limitations, as OCP-based materials demonstrate inconsistent biological effects and may exhibit cytotoxicity attributed to excessive calcium ion release into surrounding tissues [16]. Furthermore, the immunological properties of OCP remain incompletely understood. In particular, it remains unclear how simultaneously co-doping OCP with two divalent cations (e.g., Sr^{2+}/Mg^{2+} or Sr^{2+}/Ba^{2+}) affects the phagocytic activity, oxidative response, and cytokine production of monocytes and macrophages, since most existing studies have examined single-ion-doped systems rather than multi-doped formulations [12]. Clarifying these effects is essential for the rational design of next-generation immunomodulatory calcium phosphate biomaterials.

To improve the biological compatibility of OCP, various modification approaches are being proposed. Controlled doping of the OCP crystal structure with biologically active ions represents one of the most promising strategies. This modification is anticipated not only to reduce potential material cytotoxicity but also to deliberately alter its osteogenic and immunomodulatory properties. Previous research has indicated that partial substitution of Ca^{2+} ions with Sr^{2+} in OCP (from ≈ 20 at. %) contributes to reduced cytotoxicity in vitro [5,17].

Bone hydroxyapatite contains a wide spectrum of trace elements performing crucial regulatory functions. Therefore, the development of multi-substituted calcium phosphate compounds and investigation of their interactions with immune cells presents significant scientific and practical interest [18]. Considering the heteroionic composition of natural bone hydroxyapatite and the biological roles of its constituent trace elements, the creation and study of multi-substituted calcium phosphate systems represent a relevant research direction. Particular attention is devoted to divalent cations Mg^{2+} and Ba^{2+}, which not only resemble Ca^{2+} ions but also actively participate in regulating bone tissue homeostasis [19].

Thus, the objective of this work was a comprehensive investigation of the biological properties of low-temperature octacalcium phosphates doped with strontium, barium, and magnesium ions in vitro, aiming to develop a promising osteoplastic material with enhanced osteogenic and immunomodulatory characteristics.

2. Methods

2.1. Cell cultures and reagents

MG-63 human osteoblast-like cells were obtained from ATCC (Manassas, VA, USA). MycoFluor™ mycoplasma detection kit was purchased from Thermo Scientific (Waltham, MA, USA). Fetal bovine serum (FBS) (heat-inactivated) was purchased from Gibco (Gibco, Waltham, MA, USA). Cell culture media EMEM and DMEM, lyophilized bovine serum albumin (BSA), antibiotics ciprofloxacin, gentamicin sulfate, fluorescent dyes Bisbenzimide Hoechst 33342, Propidium Iodide, Calcein AM, trypan blue (C.I. 23850) and other chemicals were purchased from Sigma-Aldrich (Milwaukee, WI, USA). Antimycotic fluconazole was purchased from Pfizer (Paris, France). Cell Viability Reagent

Alamar-Blue was purchased from Invitrogen (Carlsbad, CA, USA). Ammonium dihydrogen phosphate and calcium nitrate tetrahydrate were purchased from PanReac Applichem (ITW Reagents). Sedative/muscle relaxant Xylazine was purchased from Interchemie werken De Adelaar B.V. (Venray, Netherlands). Anesthetic Zoletil was purchased from Virbac (Carros, France).

All other reagents used were of analytical reagent quality. The chemical agents were used exactly as provided. All compounds and solvents used in this study were bought commercially and used without additional purification.

2.2. Synthesis of pure and doped octacalcium phosphate powders

The synthesis of doped OCP powders was performed using a two-step method via a dicalcium phosphate dihydrate (DCPD) precursor in a buffer system (Figure 1).

DCPD was synthesized by precipitating from a buffer solution. A 1 M $CaCl_2$ solution was added to a 1.5 M sodium acetate buffer, the pH of which was adjusted to 5.5 using orthophosphoric acid. The reaction mixture was stirred for 1 hour at 250 rpm and room temperature (25 ± 2 °C) using an overhead stirrer. The resulting precipitate was filtered, washed with distilled water to remove impurity salts, and air-dried for 3–4 days.

The transformation of DCPD into OCP was achieved by hydrolyzing the obtained DCPD powder in a 1.5 M sodium acetate buffer solution. The solid-to-liquid ratio was maintained at 1:100. The reaction was carried out for at least 24 hours at 35 ± 2 °C under constant stirring. This procedure yielded pure OCP powder.

To obtain co-doped OCP powders (with Sr^{2+}/Mg^{2+} or Sr^{2+}/Ba^{2+}), the corresponding metal salts ($Sr(NO_3)_2$, $Mg(NO_3)_2$, or $Ba(NO_3)_2$) were added to the sodium acetate buffer solution during the DCPD hydrolysis step. The optimal theoretical substitution concentrations, as determined in previous studies, were 10–20 at.% for Sr^{2+} relative to Ca^{2+}, and 1, 5, 10 at.% for the secondary cations (Mg^{2+} or Ba^{2+}). For this study, samples OCP_Sr20_Mg1 and OCP_Sr20_Ba1 were synthesized. The hydrolysis was conducted for at least 48 hours at 35 ± 2 °C under constant magnetic stirring at 250 rpm. The resulting powders were filtered, washed, and air-dried.

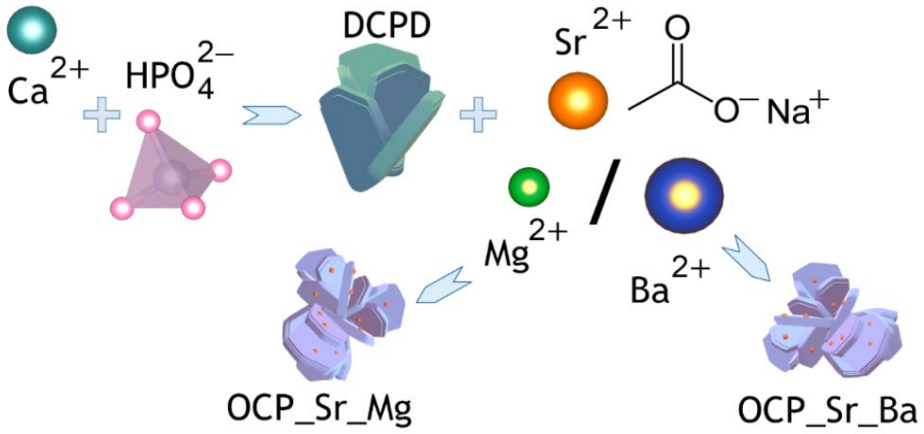

Figure 1. Synthesis methodology of dual-substituted samples: preparation of DCPD via liquid-phase synthesis followed by hydrolysis of OCP crystals in a solution containing sodium acetate, strontium, and magnesium (or barium) cations.

2.3. Phase composition analysis

The phase composition of the synthesized powders was analyzed using X-ray diffraction (XRD) on a Shimadzu XRD-6000 diffractometer equipped with an automated visualization system. The dried and sieved (< 100 μm) powders were examined. Full profile analysis of the diffraction patterns was performed using the Jana 2006 software and the JCPDS 2003 database.

2.4. Fourier-transform infrared (FT-IR) spectroscopy

Chemical functional groups were identified using a Nicolet Avatar 330 FT-IR spectrometer. The transmission spectra of dried powder samples were recorded in the range of 4000–400 cm^{-1} with a resolution of 1 cm^{-1}.

2.5. Microstructure and morphology

The microstructure and morphology of the samples were studied by scanning electron microscopy (SEM) using a TESCAN VEGA III microscope (Brno, Czech Republic). The samples were sputter-coated with gold using a Q150R Quorum Technologies coater (Lewes, UK) prior to imaging. Surface images were obtained at a column pressure of 7.3×10^{-2} Pa and a chamber pressure of 1.5×10^{-1} Pa.

2.6. Cell culture and cultivation conditions

The study utilized monoblast-like cells of the THP-1 cell line, obtained from ATCC (Wesel, Germany). The cells were cultured in a CO_2 incubator (CB53, Binder, Germany) at 37 °C in a humidified atmosphere containing 5% CO_2, using RPMI-1640 medium supplemented with 10% FBS (Gibco, USA) and 40 μg/ml gentamicin sulfate. The absence of mycoplasma contamination in the cell culture was confirmed using the MycoFluor™ kit (Thermo Scientific, USA).

THP-1ATRA monocyte-like cells were derived by treating the parental THP-1 cells with 1 μM ATRA (all-trans retinoic acid) (Merck, Hamburg, Germany) for 72 hours [20,21].

THP-1PMA macrophage-like cells were obtained by treating the parental THP-1 cells with 100 nM phorbol 12-myristate 13-acetate (PMA) for 72 hours [22]. Prior to the addition of CPCs, the THP-1PMA cells were washed three times with culture medium [22].

The phenotypic characteristics of THP-1ATRA and THP-1PMA cells were characterized in a previous study [23].

For the experiments, THP-1 cells were seeded in 96-well plates (SPL Life Sci., South Korea) at a density of 15×10^3 cells/cm^2 and subsequently differentiated into THP-1ATRA or THP-1PMA. After differentiation with ATRA or PMA was complete, the differentiation medium containing the inducer (ATRA or PMA) was completely removed and the cells were washed with culture medium to remove residual inducers. To create pro-inflammatory conditions, a portion of the differentiated cells was then treated with 10 μg/ml lipopolysaccharide (LPS) from *E. coli* O111:B4 for 24 hours, while the remaining cells were left under standard (non-activated) conditions. After LPS-treatment, the medium was removed from all wells and the cells were washed with culture medium three times. 100 μl of fresh medium (without inducer or LPS) containing pre-sterilized OCP_Sr20_Mg1 or OCP_Sr20_Ba1 at a concentration of 1 mg/ml was then added to both the non-activated and LPS-activated cells, according

to the methodology described by Teterina *et al.* [6]. The cells were co-cultured with the CPCs for 72 hours, after which the target parameters were investigated [18].

2.7. Assessment of the effect of calcium phosphate ceramics on cell viability

The viability of THP-1ATRA and THP-1PMA cells after incubation with OCP_Sr20_Mg1 and OCP_Sr20_Ba1 was assessed using the AlamarBlue reduction assay (Invitrogen, Carlsbad, CA, USA). After 72 hours of incubation with OCP_Sr20_Ba1 or OCP_Sr20_Mg1, AlamarBlue was added to the cells at a concentration of 100 µg/ml. The cells were then incubated for 4 hours at 37 °C and 5% CO_2, after which the fluorescence intensity was measured at Ex530 nm/Em595 nm using an Infinity F200 microplate spectrofluorometer (Tecan, Männedorf, Switzerland). Cell viability was evaluated based on the mean fluorescence intensity (MFI) of the resulting resorufin product.

2.8. Phagocytosis assay

Phagocytic activity was assessed by determining the percentage of phagocytic cells (phagocytic index) and the MFI of pHrodo Green *E. coli* (Fisher Scientific, Waltham, MA, USA) (phagocytic capacity) within the cells. After 72 hours of co-incubation with OCP_Sr20_Mg1 or OCP_Sr20_Ba1, the cells were treated with 1 mg/ml pHrodo Green *E. coli* (Fisher Scientific, Waltham, MA, USA) for 2 hours at 37 °C and 5% CO_2. To control for non-specific staining, a portion of the cells was pre-incubated with 10 µg/ml cytochalasin D (Merck Millipore, St. Louis, MO, USA). Measurements were performed using an Infinity F200 microplate spectrofluorometer (Tecan, Männedorf, Switzerland) at Ex485/Em530. The obtained fluorescence values were normalized to the fluorescence intensity of cell nuclei stained with Hoechst 33342 (Ex/Em: 350/461 nm).

2.9. LysoTracker staining

To assess lysosomal content, after 72 hours of culturing with OCP_Sr20_Mg1 and OCP_Sr20_Ba1, the cells were stained by adding 50 nM LysoTracker Green DND-26 (Thermo Fisher Scientific, Waltham, MA, USA) to the culture medium. Staining was performed for 30 minutes under CO_2 incubator conditions. As a positive control, cells were incubated with 50 µM chloroquine (Sigma-Aldrich, St. Louis, MO, USA) for 4 hours. Measurements were conducted using an Infinity F200 microplate spectrofluorometer (Tecan, Männedorf, Switzerland) at Ex485/Em530. The obtained fluorescence values were normalized to the fluorescence intensity of cell nuclei stained with Hoechst 33342 (Ex/Em: 350/461 nm).

2.10. ROS production assay

To assess constitutive and inducible intracellular production of reactive oxygen species (ROS), after 72 hours of culturing with OCP_Sr20_Mg1 and OCP_Sr20_Ba1, the cells were stained by adding 20 µM 2',7'-dichlorodihydrofluorescein diacetate (DCFH-DA, SI-D6883, Sigma-Aldrich, St. Louis, MO, USA) to the culture medium. Staining was performed for 15 minutes under CO_2 incubator conditions. As a positive control, cells pre-incubated with 1 mM hydrogen peroxide (Sigma-Aldrich, St. Louis, MO, USA) for 20 minutes were used. Measurements were performed using an Infinity F200

microplate spectrofluorometer (Tecan, Männedorf, Switzerland) at Ex485/Em530. The obtained fluorescence values were normalized to the fluorescence intensity of cell nuclei stained with Hoechst 33342 (Ex/Em: 350/461 nm).

2.11. Analysis of TNF-α, IL-1β, and IL-6 cytokine secretion

To analyze the secretion of pro-inflammatory cytokines (TNF-α, IL-1β, and IL-6) by monocyte-like and macrophage-like cells, the culture medium was collected after 72 hours of culturing with OCP_Sr20_Mg1 or OCP_Sr20_Ba1 powders. The medium was centrifuged at 300 × g for 5 minutes, and the supernatant was used for further analysis. The secretion of TNF-α, IL-1β, and IL-6 was evaluated using commercial ELISA kits: Interleukin-1 beta-ELISA-BEST, Interleukin-6-ELISA-BEST, and Alpha-TNF-ELISA-BEST (Vector-Best, Moscow, Russia), following the manufacturer's instructions. Optical density was measured at a wavelength of 450 nm using an iMark microplate reader (Bio-Rad, Hercules, CA, USA).

Investigation was focused on characterizing the pro-inflammatory (M1-associated) response, since LPS activation was used specifically to simulate the acute pro-inflammatory conditions typically present at the implantation site. LPS/TLR4 signaling is a canonical driver of M1, rather than M2, macrophage polarization, and the primary readout of such stimulation is the production of pro-inflammatory cytokines (TNF-α, IL-1β, IL-6) [24]. Conversely, the induction of the anti-inflammatory/M2 phenotype and the associated upregulation of IL-10, TGF-β, and CD206 is classically driven by IL-4/IL-13 signaling, rather than by LPS. Therefore, measuring M2 markers in this particular experimental setting would not be expected to reveal the functional consequences of the material's interaction with the cells under the inflammatory conditions modeled here, and would not directly address the mechanistic question posed in this study. Consequently, we limited our analysis to the pro-inflammatory arm of the response, which constitutes the biologically relevant and mechanistically interpretable outcome for our LPS-based *in vitro* model.

2.12. Statistical analysis

The results are presented as mean ± standard deviation. All experiments were performed with at least 4 replicates ($n \geq 4$).

The Mann-Whitney U test was used for comparing two independent samples.

Prior to multiple-group comparisons, data were assessed for normality and homogeneity of variances using the Shapiro–Wilk and Brown–Forsythe tests, respectively. For data that met the assumptions of normality and homogeneity of variances, one-way analysis of variance (ANOVA) was performed, followed by Tukey's multiple-comparison test. For data that did not meet the assumptions of normality, the Kruskal–Wallis H test was used, followed by Dunn's post-hoc test with Holm–Šídák correction for multiple comparisons. The magnitude of the observed effects was estimated using the standardized mean difference calculated according to Hedges' g.

Statistical analysis and visualization of the results were performed using the Python 3 programming language (version 3.13.0) in the Spyder development environment (version 5.5.1), with the Pandas (version 2.2.3), NumPy (version 1.26.4), SciPy (version 1.13.1), Matplotlib (version 3.9.2), Seaborn (version 0.13.2) and Pingouin (version 0.5.5) libraries.

3. Results

3.1. Physicochemical characteristics of doped OCP

According to the XRD results (Figure 2A), all synthesized samples were monophasic and matched the reference pattern No. 26-1056 from the ICDD database (Powder Diffraction File, Alphabetical Index Inorganic Compounds, Pennsylvania: JCPDS, 1997). The spectra of the substituted samples showed the characteristic (0 0 2) and (0 7 0) reflexes, while the remaining reflexes were overlapped due to the low degree of crystallinity of the obtained materials.

The Fourier-transform infrared spectroscopy (FTIR) spectra of the synthesized materials exhibited all characteristic modes for OCP, indicating the absence of X-ray amorphous impurities (Figure 2B). Detected bands included vibrations of phosphate groups at 561 and 602 cm^{-1} (ν_4), 962 cm^{-1} (ν_1), and 1040, 1121, and 1295 cm^{-1} (ν_3), as well as vibrations of the hydrogen phosphate group at 861 and 916 cm^{-1}. Carbonate modes at 1452 and 1558 cm^{-1} were also observed, consistent with findings reported in a previous study [19].

The samples retained the original lamellar crystalline form of the DCPD precursor. However, the surfaces were additionally covered with newly formed, fine needle-like OCP crystals (Figure 2C,D).

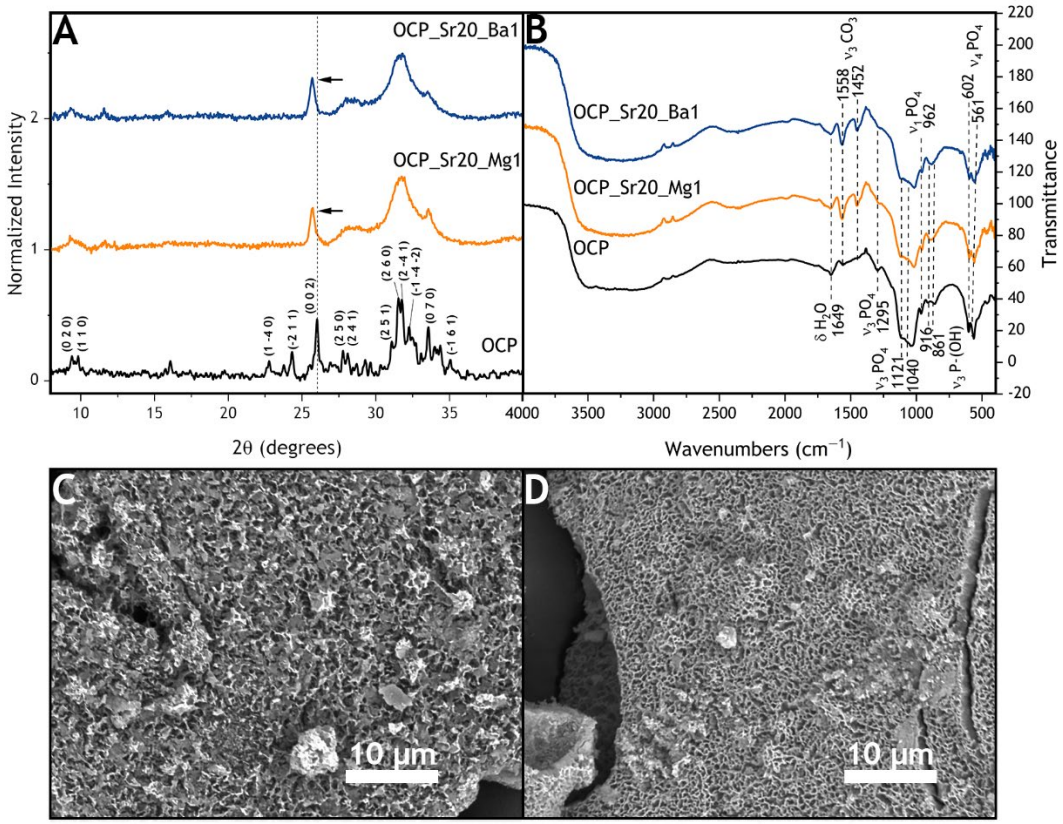

Figure 2. Physico-chemical characteristics of OCP. **(A)** XRD patterns and **(B)** FTIR spectra of pure OCP and its substituted analogues; SEM images of the OCP_Sr20_Mg1 **(C)** and OCP_Sr20_Ba1 **(D)** samples.

XRD analysis is a widely used method for investigating the long-range order in crystals. The reflections in Figure 2A are poorly resolved; the overlapping peaks on the diffractogram result from the low degree of crystallinity of the substituted materials, characterized by small crystallite sizes and a

significant amount of amorphous phase. The crystallite size can be estimated approximately using Scherrer's formula (Table 1):

$$D = \frac{k\lambda}{\beta cos\theta} \quad (1)$$

where D—crystallite size [nm], λ—wavelength of irradiation (for CuK_α $\lambda = 1.54056$ Å) [Å], $cos\theta$—Bragg angle [°], k—shape factor (k = 1 in our case), β—full width at half maximum.

Table 1. Approximate crystallite size for samples, calculated using Equation (1) for peaks (0 0 2) and (0 7 0).

	OCP	OCP_20Sr_1Mg	OCP_20Sr_1Ba
Crystallite size [nm]	64.68 ± 2.41	34.73 ± 2.65	35.24 ± 1.96

The incorporation of strontium cations into the OCP structure is evidenced by the shift of the (0 0 2) plane peak towards lower angles, indicating an increase in interplanar distances. This observation is consistent with the larger ionic radius of the Sr^{2+} cation compared to Ca^{2+}.

Consequently, the introduction of strontium destabilizes the crystalline structure of OCP, leading to a reduction in crystallite size and an increase in the concentration of the X-ray amorphous phase, which is characteristic of this type of ionic substitution [25]. The influence of the additional barium and magnesium cations is difficult to ascertain due to the poor resolution of the corresponding peaks.

3.2. Cytotoxicity assessment of doped octacalcium phosphate

The viability of THP-1ATRA monocyte-like cells and THP-1PMA macrophage-like cells was evaluated following 72 hours of incubation with 1 mg/mL of either OCP_Sr20_Ba1 or OCP_Sr20_Mg1 (Figure 3). The results demonstrated that none of the investigated CPCs exhibited cytotoxic effects under either standard or pro-inflammatory culture conditions. The cell viability of both THP-1ATRA and THP-1PMA cells remained above 90% after incubation with all tested CPCs.

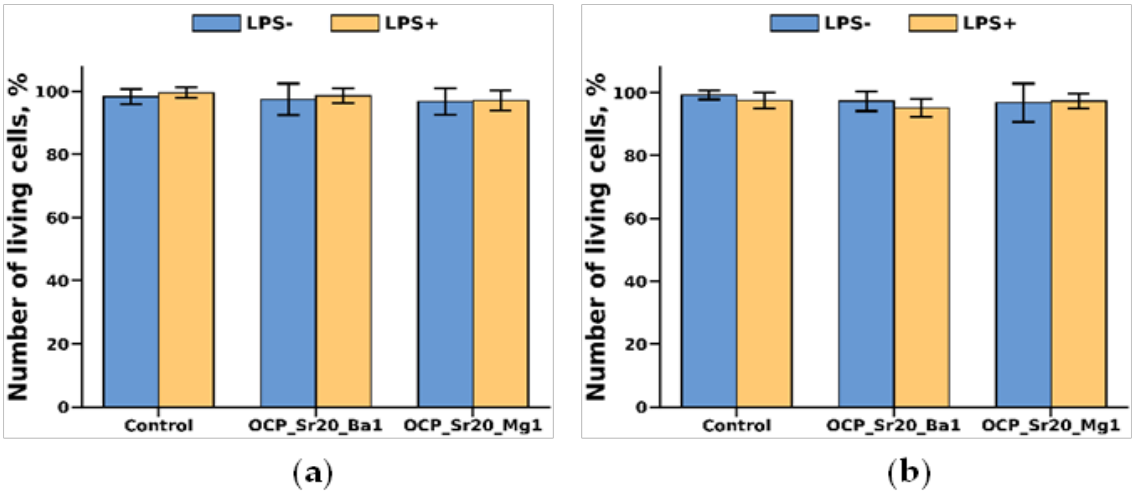

Figure 3. Viability of THP-1ATRA monocyte-like cells and THP-1PMA macrophage-like cells after 72-hour incubation with 1 mg/mL of OCP_Sr20_Mg1 or OCP_Sr20_Ba1. **(a)** ATRA; **(b)** PMA. Data are presented as mean ± standard deviation (n ≥ 4).

3.3. Investigation of the effect of doped octacalcium phosphate on phagocytic activity

The phagocytic activity of monocyte-like and macrophage-like cells was assessed by measuring the phagocytic index and phagocytic number (Figure 4). It was found that none of the investigated CPCs affected the phagocytic index of THP-1 ATRA monocyte-like cells under either standard or pro-inflammatory culture conditions.

Analysis of the phagocytic number revealed that under standard conditions, OCP_Sr20_Ba1 statistically significantly increased the phagocytic activity of THP-1ATRA monocyte-like cells to 172.9% ± 11.1% relative to the control, whereas OCP_Sr20_Mg1 had no significant effect (105.0% ± 12.3%).

Under pro-inflammatory conditions, both calcium phosphate materials significantly enhanced phagocytic activity compared to standard conditions. OCP_Sr20_Ba1 demonstrated a more pronounced effect (328.3% ± 30.6% relative to control) compared to OCP_Sr20_Mg1 (270.2% ± 25.6%).

In THP-1 PMA macrophage-like cells, both calcium phosphate materials reduced the phagocytic number to the level induced by cytochalasin D (62.5% ± 11.4%), under both standard and pro-inflammatory culture conditions.

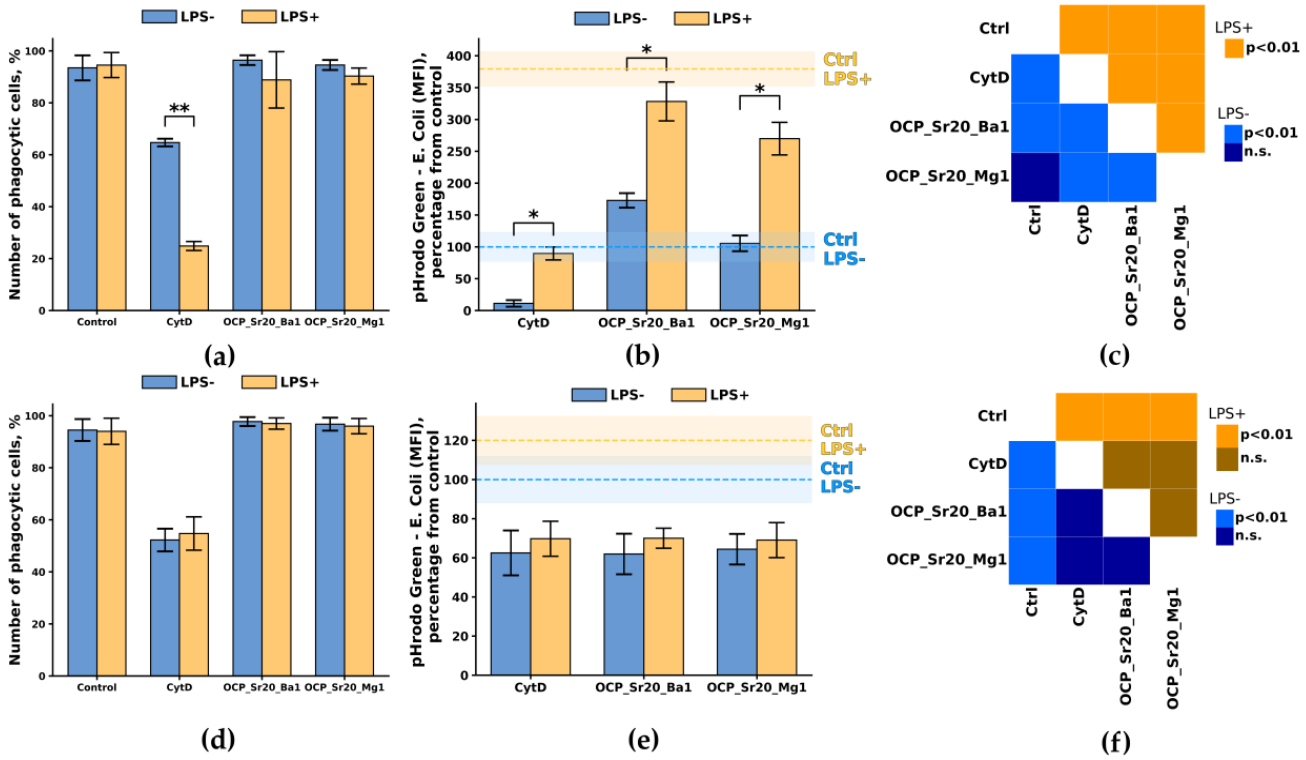

Figure 4. Effect of OCP_Sr20_Ba1 and OCP_Sr20_Mg1 on the phagocytic index of THP-1 ATRA monocyte-like cells and THP-1 PMA macrophage-like cells after 72-hour incubation. Data are presented as mean ± SD (n ≥ 4); *—p<0.05 (Mann-Whitney U test). C—control; CytD—cytochalasin D. Results of one-way ANOVA with post-hoc Tukey test for the effect of OCP_Sr20_Mg1 and OCP_Sr20_Ba1 on the phagocytic number of THP-1 ATRA monocyte-like cells and THP-1 PMA macrophage-like cells (n ≥ 4). **(a)** ATRA Phagocytic Index; **(b)** ATRA Phagocytic Number; **(c)** ATRA Phagocytic Number Matrix; **(d)** PMA Phagocytic Index; **(e)** PMA Phagocytic Number; **(f)** PMA Phagocytic Number Matrix.

3.4. Investigation of the effect of doped octacalcium phosphate on acidic compartment content

Investigation of the effect of doped OCP on acidic compartment content revealed that incubation of THP-1 ATRA monocyte-like cells with OCP_Sr20_Ba1 and OCP_Sr20_Mg1 under standard conditions led to a reduction in the number of acidic compartments to 62.2% ± 5.4% and 51.7% ± 8.6% of the control, respectively (Figure 5). Under pro-inflammatory conditions, a decrease in acidic compartment content was also observed to 86.8% ± 5.0% for OCP_Sr20_Ba1 and 83.6% ± 4.3% for OCP_Sr20_Mg1 relative to the control; however, these differences were not statistically significant.

In THP-1 PMA macrophage-like cells, no statistically significant changes in acidic compartment content were observed after incubation with either CPC, under both standard and pro-inflammatory conditions.

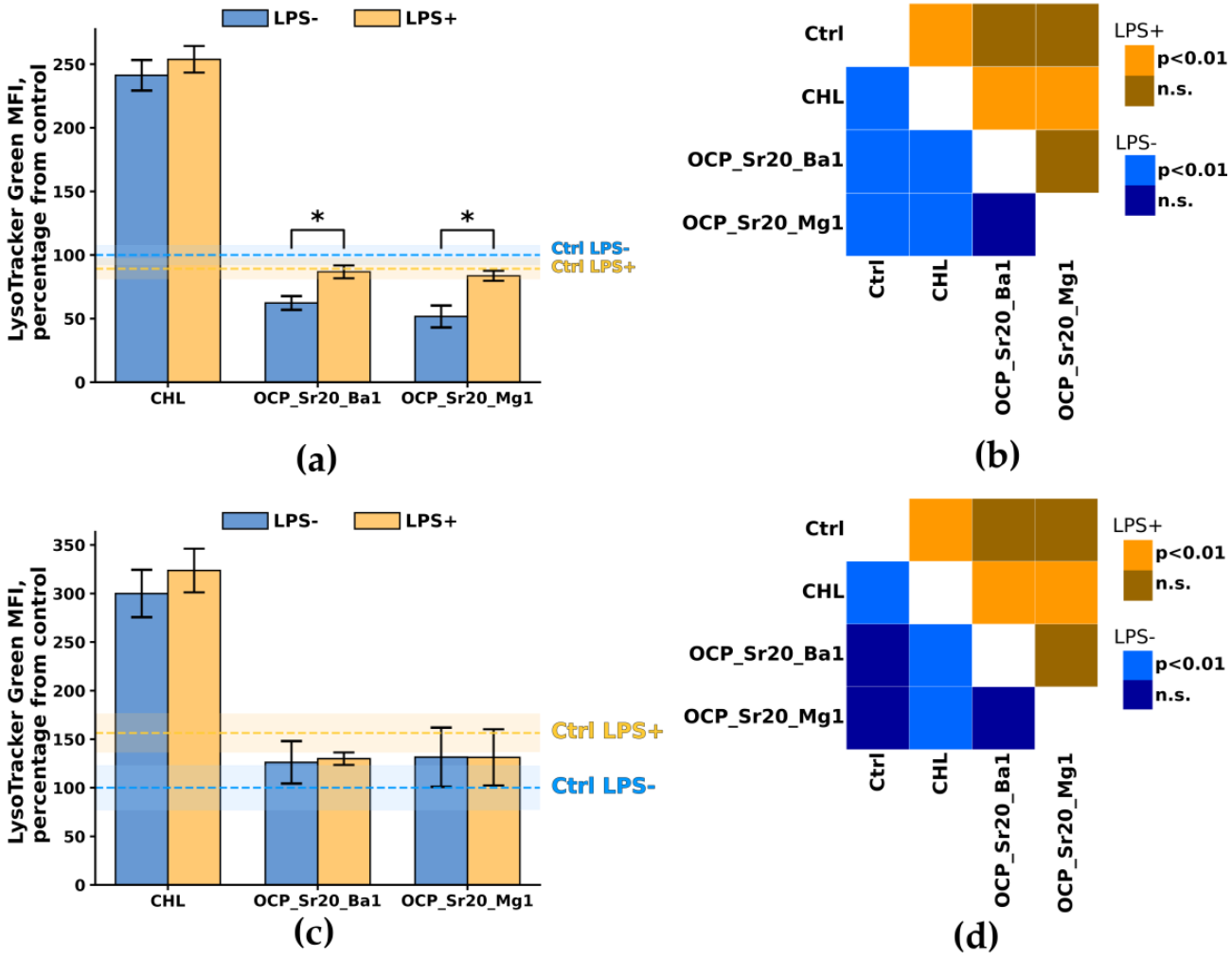

Figure 5. Effect of OCP_Sr20_Ba1 and OCP_Sr20_Mg1 on acidic compartment content in **(a, b)** THP-1 ATRA monocyte-like cells and **(c, d)** THP-1 PMA macrophage-like cells after 72-hour incubation. Data are presented as mean ± SD (n ≥ 4); *—p < 0.05 (Mann-Whitney U test). Ctrl—control; CytD—cytochalasin D. Results of one-way ANOVA with posthoc Tukey test for the effect of OCP_Sr20_Mg1 and OCP_Sr20_Ba1 on the phagocytic number of THP-1 ATRA monocyt-like cells and THP-1 PMA macrophage-like cells (n ≥ 4). **(a)** ATRA Acidic Compartment Content; **(b)** ATRA Acidic Compartment Content Comparative Matrix; **(c)** PMA Acidic Compartment Content; **(d)** PMA Acidic Compartment Content Comparative Matrix.

3.5. Investigation of the effect of doped octacalcium phosphate on ROS production

The investigation into the effect of doped OCP forms on ROS production revealed that under standard culture conditions, the studied CPCs did not affect ROS production by ATRA monocyte-like cells (Figure 6). In contrast, under pro-inflammatory conditions, a reduction in ROS production was observed for both OCP_Sr20_Ba1 and OCP_Sr20_Mg1, to 51.8% ± 4.0% and 51% ± 4.2% of the control level, respectively.

In PMA macrophage-like cells under standard conditions, the calcium phosphate materials induced an increase in ROS production to 131.9% ± 4.4% for OCP_Sr20_Ba1 and 150.4% ± 3.1% of the control for OCP_Sr20_Mg1. Under pro-inflammatory conditions, OCP_Sr20_Ba1 decreased ROS production compared to the LPS-treated control, whereas OCP_Sr20_Mg1 increased it.

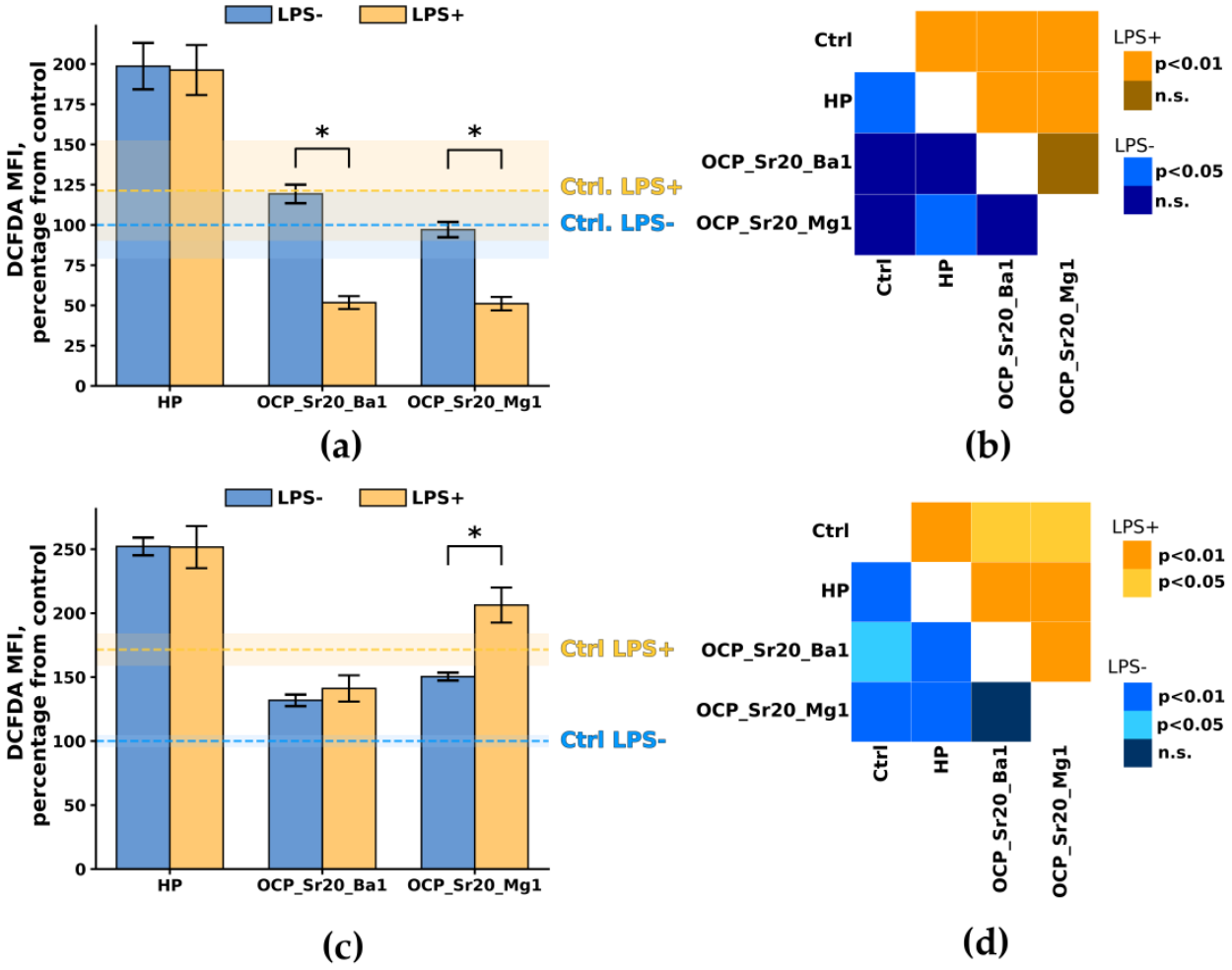

Figure 6. Effect of OCP_Sr20_Mg1 and OCP_Sr20_Ba1 on constitutive and inducible intracellular reactive oxygen species production in **(a, b)** THP-1 ATRA monocyte-like cells and **(c, d)** THP-1 PMA macrophage-like cells after 72-hour incubation. Data are presented as mean ± SD (n ≥ 4); *—$p < 0.05$; n.s.—not statistically significant (Mann-Whitney U test). HP—hydrogen peroxide. ATRA LPS−: Kruskal-Wallis H-test with Dunn's post hoc test with Holm–Šídák correction; ATRA LPS +: One-way ANOVA with post-hoc Tukey test. **(a)** ATRA ROS production; **(b)** ATRA ROS production Comparative Matrix; **(c)** PMA ROS production; **(d)** PMA ROS production Comparative Matrix.

3.6. Investigation of the effect of doped octacalcium phosphate on the production of pro-inflammatory cytokines TNF-α, IL-1β, and IL-6

Analysis of the effects of the doped OCP forms revealed that both investigated calcium phosphate materials (OCP_Sr20_Mg1 and OCP_Sr20_Ba1) substantially enhanced the production of pro-inflammatory cytokines by THP-1 monocyte-like cells under both standard and pro-inflammatory conditions, albeit with differential effects on specific cytokines. Under standard culture conditions, OCP_Sr20_Mg1 induced a less pronounced increase in TNF-α (46.8 ± 3.6 pg/ml) and IL-1β (221.0 ± 3.7 pg/ml) levels compared to OCP_Sr20_Ba1 (103.2 ± 1.7 pg/ml and 274.2 ± 21.5 pg/ml, respectively). In contrast, under pro-inflammatory conditions, OCP_Sr20_Mg1 stimulated a stronger secretion of IL-1β (263 ± 3.9 pg/ml). Both materials increased TNF-α levels to a similar extent under pro-inflammatory conditions and enhanced IL-6 levels regardless of the culture conditions.

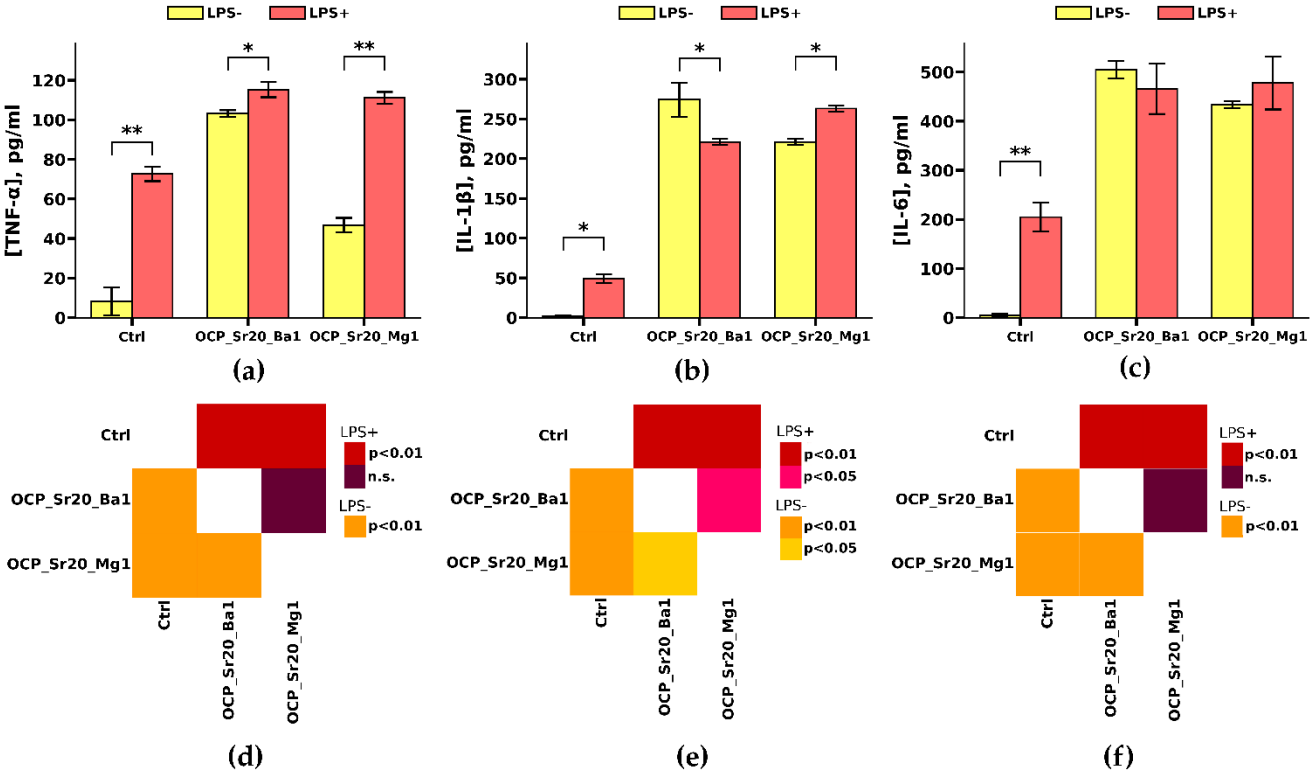

Figure 7. Effect of OCP_Sr20_Mg1 and OCP_Sr20_Ba1 on constitutive and inducible production of pro-inflammatory cytokines [TNF-α] **(a)**, [IL-1β] **(b)** and [IL-6] **(c)** by THP-1 ATRA monocyte-like cells after 72-hour incubation. Data are presented as mean ± SD (n ≥ 4); *—p < 0.05 (Mann-Whitney U test). Results of multiple comparisons of the effect of OCP_Sr20_Mg1 and OCP_Sr20_Ba1 on constitutive and inducible production of pro-inflammatory cytokines [TNF-α] **(d)**, [IL-1β] **(e)** and [IL-6] **(f)** by THP-1 ATRA monocyte-like cells (n ≥ 4). n.s.—not statistically significant. ATRA LPS: Kruskal-Wallis H-test with Dunn's post hoc test with Holm–Šídák correction; ATRA LPS +: One-way ANOVA with post-hoc Tukey test.

THP-1 PMA macrophage-like cells exhibited a less pronounced cytokine response compared to monocyte-like cells. Under standard culture conditions, both investigated materials enhanced the production of pro-inflammatory cytokines. Specifically, OCP_Sr20_Ba1 increased TNF-α levels to

414.5 ± 18.5 pg/ml compared to the control (Figure 8a). OCP_Sr20_Ba1 also elevated IL-6 to 646.1 ± 12.8 pg/ml and IL-1β to 825.6 ± 20.5 pg/ml, while OCP_Sr20_Mg1 increased the concentrations of these cytokines to 671.13 ± 101.2 pg/ml and 810.7 ± 91.4 pg/ml, respectively.

Under pro-inflammatory conditions, only OCP_Sr20_Mg1 induced a statistically significant increase in TNF-α levels (382 ± 10.4 pg/ml) compared to the control (Figure 8a). In contrast, neither of the investigated CPCs affected the production of IL-6 or IL-1β under pro-inflammatory conditions.

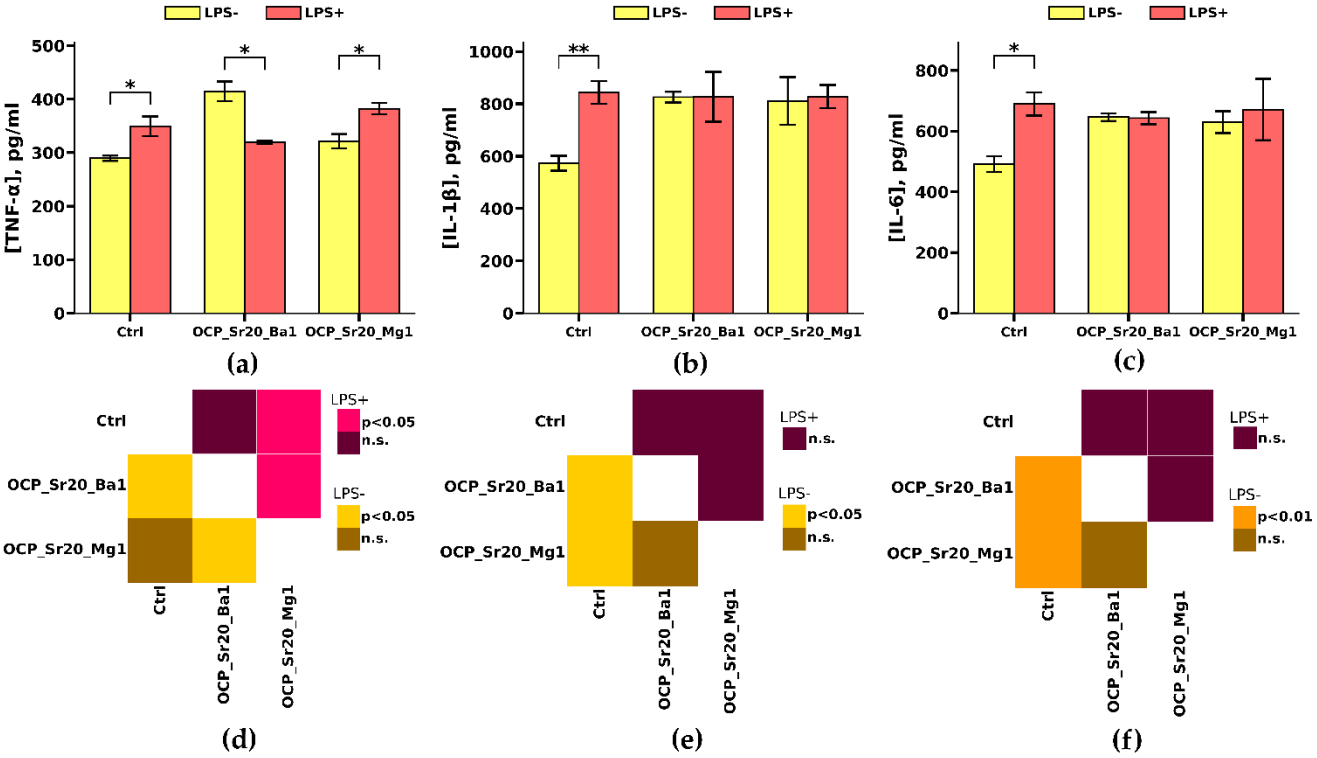

Figure 8. Effect of OCP_Sr20_Mg1 and OCP_Sr20_Ba1 on constitutive and inducible production of pro-inflammatory cytokines [TNF-α] **(a)**, [IL-1β] **(b)** and [IL-6] **(c)** by THP-1 PMA macrophage-like cells after 72-hour incubation. Data are presented as mean ± SD (n ≥ 4); *—p < 0.05 (Mann-Whitney U test). Results of one-way ANOVA with post-hoc Tukey test for the effect of OCP_Sr20_Mg1 and OCP_Sr20_Ba1 on constitutive and inducible production of pro-inflammatory cytokines [TNF-α] **(d)**, [IL-1β] **(e)** and [IL-6] **(f)** by THP-1 PMA macrophage-like cells (n ≥ 4). n.s.—not statistically significant.

To assess the observed biological effects, Hedges' g criterion was used to compare parameters both against the control and between different CPCs. The results demonstrate differences in cellular responses depending on both the type of calcium phosphate material and the cell type investigated. The obtained results are presented in summary tables (Figure 9).

Analysis of the CPCs' effect on intracellular compartments revealed that under pro-inflammatory conditions, they reduced both phagocytic activity and ROS production in both monocyte-like and macrophage-like cells. The most pronounced effect of all investigated CPCs was the enhancement of pro-inflammatory cytokine production by monocytes, observed under both standard and pro-inflammatory conditions. In contrast, macrophage-like cells significantly increased the secretion of pro-inflammatory cytokines only under standard culture conditions.

A comparison of OCP_Sr20_Ba1 and OCP_Sr20_Mg1 revealed several differences. In monocyte-like cells, OCP_Sr20_Mg1 reduced phagocytic activity, acidic compartment content, and ROS production under standard conditions. Furthermore, it decreased the secretion of pro-inflammatory cytokines under standard conditions but significantly increased IL-1β levels under pro-inflammatory conditions compared to OCP_Sr20_Ba1.

In macrophage-like cells, both CPCs did not substantially affect most parameters, except for ROS production, where OCP_Sr20_Mg1 demonstrated higher values. It was also noted that OCP_Sr20_Mg1 reduced TNF-α production under standard conditions but enhanced it under pro-inflammatory conditions.

		THP-1 ATRA		THP-1 PMA	
Group	**Parameter**	**LPS-**	**LPS+**	**LPS-**	**LPS+**
OCP_Sr20_Ba1	Acidic compartments	-4.99	-0.32	1.02	-1.56
OCP_Sr20_Mg1	Acidic compartments	-5.19	-0.77	1.02	-0.88
OCP_Sr20_Ba1	Phagocytic number	3.51	-1.53	-3.08	-4.79
OCP_Sr20_Mg1	Phagocytic number	0.26	-3.61	-3.2	-4.28
OCP_Sr20_Ba1	ROS	1.1	-2.75	6.18	-2.34
OCP_Sr20_Mg1	ROS	-0.17	-2.77	11.45	2.33
OCP_Sr20_Ba1	[IL-1β]	15.6	31.62	9.37	-0.2
OCP_Sr20_Mg1	[IL-1β]	68.85	34.99	2.85	-0.32
OCP_Sr20_Ba1	[IL-6]	33.4	5.43	6.7	-1.34
OCP_Sr20_Mg1	[IL-6]	67.52	5.48	3.88	-0.21
OCP_Sr20_Ba1	[TNF-α]	16.08	9.95	8.03	-2.02
OCP_Sr20_Mg1	[TNF-α]	5.97	10.03	2.7	1.91

(a)

	THP-1 ATRA		THP-1 PMA	
Parameter	**LPS-**	**LPS+**	**LPS-**	**LPS+**
Acidic compartments	-1.28	-0.6	0.17	0.06
Phagocytic number	-4.95	-1.8	0.24	-0.12
ROS	-3.65	-0.14	4.16	4.69
[IL-1β]	-3.52	11.19	-0.19	0.01
[IL-6]	-4.5	0.2	-0.53	0.34
[TNF-α]	-21.44	-1.29	-5	7.17

(b)

Figure 9. Comparative table of the magnitudes of observed biological effects, calculated using the standardized mean difference (Hedges' *g* coefficient). Effects were assessed relative to the control **(a)**, and for OCP_Sr20_Mg1 compared to OCP_Sr20_Ba1 **(b)**. An absolute Hedges' *g* coefficient value of $|*g*| \geq 1$ indicates a significant effect. Green – Parameter increase; Red: Parameter decrease; Blue: No significant effect.

4. Discussion

The incorporation of Sr^{2+}, Mg^{2+}, and Ba^{2+} into the OCP crystal lattice causes various distortions due to differences in ionic radii and coordination preferences. Strontium, which has an ionic radius larger than calcium (1.18Å for Sr^{2+} against 1.00Å for Ca^{2+}), is isomorphically substituted in the OCP structure, causing a linear expansion of the unit cell and a significant decrease in crystallinity, especially at higher substitution levels, what we can observe in Figure 2. In OCP strontium ion occupies specific cationic sites such as M(3), M(4), and M(8), leading to lattice distortion [26,27]. This structural deformation increases the solubility of the material, as the larger ion destabilizes the crystal [28]. Magnesium ion (0.72 Å) is significantly smaller and inhibits the transformation of precursor phases

into OCP, resulting in the formation of more amorphous or poorly crystalline phases [29]. Incorporation of Ba^{2+}, in addition to lattice expansion, has been shown to stabilize the structure of β-TCP, although its effect on OCP crystallinity is less well understood; however, it is known to alter particle morphology and reduce cytotoxicity at certain concentrations [30].

Changes in crystallinity and lattice deformation caused by ion substitution directly influence crystal size, shape, and surface topography, which are critical factors determining macrophage mechanotransduction. Strontium substitution in OCP leads to the formation of crystals with reduced size, damaged end groups, and jagged edges, promoting an asynchronous and less organized regeneration front [26,31]. Similarly, in dicalciumphosphate dihydrate, increased strontium content leads to crystal aggregation, indented edges, and detachment, altering the surface topography encountered by cells [32]. Macrophages are known to respond to the size, shape, and surface roughness of biomaterials, with jagged or sharp crystals causing impaired phagocytosis and a sustained proinflammatory response. Thus, the altered crystalline morphology of OCP_20Sr_1Mg compared to OCP_20Sr_1Ba will engage different mechanosensitive pathways, influencing macrophage polarization. Furthermore, surface charge modifications resulting from ion substitution influence protein corona formation, further modulating macrophage recognition and response. For example, strontium-containing biomaterials are known to promote macrophage polarization toward the anti-inflammatory M2 phenotype, which supports tissue regeneration [33,34].

In addition to the physicochemical properties of the crystals, the released ions themselves have direct and opposing effects on macrophage function. Mg^{2+} is known to promote the formation of the anti-inflammatory M2 macrophage phenotype, which supports tissue regeneration. Mechanistically, Mg^{2+} enters cells through TRPM7 channels, activating the PI3K-AKT1 pathway, which inhibits TLR4 and NF-κB signaling and reduces the levels of proinflammatory cytokines such as TNF-α, IL-1β, and IL-6 [33]. At concentrations of approximately 4.1 mM, Mg^{2+} effectively induces a transition to the M2 phenotype by increasing the expression of CD206 and anti-inflammatory cytokines while simultaneously reducing M1 markers. This Mg^{2+}-mediated immunomodulation creates a pro-regenerative environment essential for bone healing [35]. In contrast, Ba^{2+} is generally toxic to immune cells. Barium nanoparticles have been shown to reduce the viability of mononuclear phagocytes, increase superoxide release, reduce intracellular calcium release, and induce apoptosis [36]. Barium blocks K^+ channels, disrupting ion homeostasis and leading to cellular stress. Thus, while Mg^{2+} actively promotes macrophage healing, Ba^{2+} induces cytotoxicity and inflammatory stress, explaining the opposing biological effects of OCP_20Sr_1Mg and OCP_20Sr_1Ba. The combination of altered crystal-mediated mechanotransduction and direct ion-specific signaling ultimately determines macrophage response and the success of bone tissue regeneration. The dual action of the Sr^{2+} ion itself, simultaneously promoting osteogenesis and inhibiting osteoclastogenesis, further complicates this interaction, making specific ion substitution a critical factor in materials design [37,33].

As central effectors of the immune response, monocytes and macrophages determine the cellular and tissue reaction to an implanted material through changes in their functional state. The phagocytosis of material particles by monocytes and macrophages plays a key role in altering their functional state, thereby shaping the pro-regenerative or pro-inflammatory microenvironment they create. This process is mediated by the physicochemical transformation of the implant within the biological environment, including dissolution, ion exchange, and changes in the material's surface properties. For instance, a

CP implant, through dissolution/re-precipitation processes, provides a local increase in Ca^{2+} ion concentration, which chemoattracts monocytes to the wound site. These monocytes can subsequently differentiate into macrophages and, if unable to phagocytose large particles due to their size, may activate cell fusion mechanisms, forming foreign body giant cells [38]. Notably, Ca^{2+} is a modulator of this process, binding to Soluble NSF Attachment protein REceptors (SNAREs) [38].

Given the importance of phagocytosis, we investigated the influence of OCP_Sr20_Ba1 and OCP_Sr20_Mg1 on the phagocytic activity of cells. Our data indicate that the studied CP materials reduced the phagocytic activity of LPS-activated monocyte-like cells, as well as macrophage-like cells, regardless of culture conditions. Considering that Ca^{2+} is essential for normal phagocytosis, the observed suppression of phagocytic activity appears unrelated to increased divalent ion concentration from particle dissolution. Instead, it may be linked to the slow intracellular dissolution of phagocytosed CaP particles, potentially inhibiting further phagocytosis of *E. coli* [39].

Interestingly, the investigated CP materials differentially affected phagocytosis in non-LPS-activated monocyte-like cells. OCP_Sr20_Ba1 enhanced the phagocytosis of *E. coli*, whereas OCP_Sr20_Mg1 had no effect. This phenomenon may be related to the inherently lower baseline phagocytic activity of non-activated monocytes compared to activated monocytes and macrophages. The ionic composition of the doped OCP did not appear to directly influence the phagocytosis of the particles themselves.

Given that one of the primary mechanisms for degrading CP materials is their dissolution within acidic intracellular compartments (endosomes and lysosomes), we next examined the effect of doped OCP on their content [13]. Acidic compartment (lysosomal) status is closely linked to the cellular inflammatory response, since disruption of lysosomal integrity and function is a well-established trigger of inflammatory cascades, including NLRP3 inflammasome activation, making the study of acidic compartments important for understanding the material's mechanism of action. We therefore used LysoTracker-based quantification of overall acidic compartment content in the cells as a general readout of lysosomal status following exposure to doped OCP.

It should be emphasized that in the present study phagocytic activity was assessed functionally using pHrodo Green-labeled *E. coli* as the phagocytic target, *i.e.*, we measured how co-incubation with OCP affected the cells' capacity to phagocytose bacteria, rather than directly tracking the phagocytosis or intracellular fate of the OCP particles themselves. Direct tracking of the intracellular fate of OCP particles using fluorescent labeling would, in principle, allow the distribution and degradation status of the particles to be followed over time, providing a more direct causal link between phagocytosis, particle degradation and acidic compartment content, and the resulting changes in other intracellular parameters. However, stable fluorescent labeling of calcium phosphate particles is itself a non-trivial task: physically adsorbed or co-precipitated dyes are prone to leakage and dissociation from the particle surface during cell culture, which can be misinterpreted as intracellular particle distribution, and reliable tracking generally requires covalent conjugation of the dye to the particle surface via dedicated surface chemistry (e.g., silica-shell coating followed by click chemistry) [40,41]. It should also be noted that the OCP particles used in this study are considerably larger than the size range typically associated with efficient, whole-particle phagocytosis (roughly sub-micron to a few micrometers); given their micron-scale crystallite aggregates, large-scale internalization of intact particles by monocyte-like and macrophage-like cells is unlikely, although smaller particles or fragments generated during synthesis or dissolution may still be phagocytosed, and tracking the intracellular

dynamics of such smaller fragments remains an interesting question for future work [42,43]. Importantly, OCP may influence phagocytic and other intracellular immune functions not only through direct uptake of particles, but also via interaction with the cell membrane, extracellular dissolution and ion release, and other mechanisms that do not require internalization of the material itself. In the context of implant materials specifically, we consider that such cell-material interface interactions, rather than complete engulfment of bulk particles, are likely to play the key role in shaping the immunomodulatory response, consistent with the concept that biomaterial surfaces predominantly engage phagocytes through receptor-mediated contact and, for non-internalizable material, through frustrated-phagocytosis-like mechanisms at the surface [44].

According to our data, an increase in acidic compartment content was observed only in non-activated macrophage-like cells, whereas the effect was less pronounced in monocyte-like cells. This phenomenon may presumably be related to the intracellular transformation of the doped OCP occurring within the acidic lysosomal environment. Interestingly, additional LPS stimulation of macrophages did not increase acidic compartment content. It appears that pre-activation of macrophages with LPS alters their intracellular processes such that subsequent exposure to CP suppresses lysosome formation. It is known that LPS induces lysosome tubulation in macrophages, regulated by mTOR, whose activity is itself dependent on calcium signaling [45–47]. Furthermore, macrophages exposed to particles can develop progressive lysosomal destabilization, leading to NALP3 inflammasome activation [48]. These factors may collectively contribute to the reduced acidic compartment content observed in activated macrophage-like cells.

ROS play a crucial role in cellular signaling and physiological processes; however, their excessive production leads to oxidative stress, associated with various pathological conditions. In the context of bone regeneration, elevated ROS levels promote macrophage polarization towards the pro-inflammatory M1 phenotype and activate osteoclasts, shifting the balance towards bone resorption [49,50].

Our results demonstrate a differential influence of the investigated CaP materials on ROS production. In monocyte-like cells, the materials had a minimal effect on ROS generation under standard conditions but reduced its level under pro-inflammatory conditions. In macrophage-like cells, increased ROS production was observed under standard conditions, whereas under pro-inflammatory conditions, Ba^{2+}-doping reduced and Mg^{2+}-doping increased ROS levels.

It is known that Sr^{2+} and Mg^{2+} ions possess antioxidant properties, presumably by regulating the activity of antioxidant enzymes [51–53]. Our previous research showed that Sr-doped OCP could reduce ROS production in mesenchymal cells in a dose-dependent manner [5]. Similarly, an Mg^{2+}-containing hydrogel was shown to promote bone regeneration in osteoporosis by neutralizing ROS and modulating immunity [54]. Furthermore, Jin *et al.* demonstrated that biodegradation products of an Mg^{2+}-containing alloy reduced ROS production in THP-1-derived macrophage-like cells via the TRPM7–PI3K–AKT1 signaling axis [55]. However, these findings were obtained using material extracts and did not account for the direct contact between particles and cells. In this context, the work by Kim J *et al.* is relevant, where direct interaction with particles of an Mg-containing alloy showed neither a reduction in ROS levels nor stimulation of cell proliferation, highlighting the critical importance of considering not only the ionic composition but also the direct interaction of the material with cells [56].

Information regarding the influence of Ba^{2+} on oxidative stress is limited. The cytotoxic effects of Ba^{2+} are thought to be related to its blockade of potassium channels in the cell membrane, promoting the influx of K^+ [57]. However, incorporating small amounts of Ba^{2+} into osteoplastic materials does not enhance their cytotoxicity [58]. We have previously shown that even 1% Ba^{2+} doping in OCP can suppress ROS production under pro-inflammatory conditions [59]. Therefore, it is likely that ROS production by cells following incubation with doped OCP is determined by a complex of physicochemical properties affecting its interaction with cells, rather than solely by its ionic composition. Since Ba^{2+} is clinically recognized as potentially myotoxic, our short-term *in vitro* cytotoxicity data are not sufficient to fully exclude long-term toxic effects, and longer-term cytotoxicity assessment together with *in vivo* toxicity data represent an important next step before clinical application [60].

Acute and chronic inflammatory processes are characterized by increased production of pro-inflammatory cytokines such as TNF-α, IL-1β, and IL-6, which play a dual role in bone regeneration. On one hand, these mediators are necessary for initiating the primary inflammatory response and triggering reparative processes; their secretion dynamics and concentration largely determine the fate of the implant. On the other hand, excessive or prolonged production disrupts the bone remodeling balance by stimulating osteoclast activity via RANKL-dependent mechanisms and suppressing the osteogenic differentiation of mesenchymal stem cells [61,62]. The functional consequences of a given cytokine profile cannot be reliably predicted based on its concentration alone: the resulting biological effect depends on multiple interacting factors, such as concentration, duration of exposure, and, crucially, the specific combination of cytokines present. It should be noted that proinflammatory cytokines themselves are not detrimental to bone regeneration; for example, transient TNF-α signaling is actually required for normal fracture healing, as TNF receptor-deficient mice exhibit impaired endochondral and intramembrane bone formation [63], and TNF-α, acting synergistically with IL-1β, promotes matrix mineralization by mesenchymal stem cells and is required for bone regeneration *in vivo* [64] Similarly, IL-6, despite being a classic proinflammatory cytokine, is required for normal bone callus formation and mineralization, as IL-6-deficient mice exhibit delayed fracture healing [65]. These examples demonstrate that specific combinations and temporal patterns of proinflammatory cytokines, rather than their mere presence or absolute concentration, determine whether the resulting response promotes regeneration or resorption.

In this study, we deliberately focused on characterizing the pro-inflammatory (M1-associated) response, since LPS activation was used specifically to simulate the acute pro-inflammatory conditions typically present at the implantation site, and LPS/TLR4 signaling is a canonical driver of M1, rather than M2, macrophage polarization [66]. Induction of the anti-inflammatory/M2 phenotype, and the associated upregulation of IL-10, TGF-β, and CD206, is instead classically driven by IL-4/IL-13 signaling rather than by LPS [25], and would not necessarily be expected under the pro-inflammatory conditions modeled here.

Investigating the influence of multi-doped CP materials on pro-inflammatory cytokine production revealed their pronounced stimulatory effect on monocyte-like cells, observed irrespective of culture conditions. Under standard conditions, monocyte-like cells demonstrated the highest production of pro-inflammatory cytokines relative to the control, with OCP_Sr20_Ba1 exerting a more pronounced effect on TNF-α secretion compared to OCP_Sr20_Mg1. Majumdar *et al.* showed that Ba^{2+}-doped bioactive glass exhibited an anti-inflammatory effect and reduced the production of

pro-inflammatory cytokines, including TNF-α, in glioblastoma cells, an effect possibly linked to released Ba^{2+} ions [67]. The enhanced TNF-α production by monocyte-like cells observed in our study is likely governed by a fundamentally different mechanism, namely the specific nature of the direct interaction between the material particles and the cell surface.

Interestingly, the investigated CP materials enhanced the production of IL-6 and IL-1β cytokines only in non-activated macrophage-like cells and had no effect on their production in LPS-activated macrophage-like cells. Notably, the production of IL-1β by activated macrophage-like cells correlates well with the effect of CP on acidic compartment content. This phenomenon aligns with literature data: for instance, one study showed that in macrophages loaded with palmitate and stimulated with LPS, NLRP3 inflammasome activation occurs via a lysosome-dependent mechanism [68]. Furthermore, disruptions in lysosomal calcium regulation led to reduced pro-IL-1β levels and, consequently, decreased secretion of mature IL-1β. Our data indirectly suggest that phagocytosis and intracellular degradation of CP particles induce changes in calcium homeostasis that can modulate the inflammatory response.

It is also noteworthy that in non-activated macrophage-like cells, Ba^{2+}-doping enhanced the production of the key pro-inflammatory cytokine TNF-α, whereas in activated cells, Mg^{2+}-doping enhanced it. Mg^{2+} ions are generally considered anti-inflammatory agents, and several studies report Mg^{2+}-mediated suppression of pro-inflammatory cytokine secretion. For example, Sun *et al.* demonstrated that extracts from biodegradable magnesium microparticles exhibited an anti-inflammatory effect by promoting macrophage differentiation from the M0 to the M2 phenotype, with the observed effects attributed to Mg^{2+}-induced reduction in NF-κB activation [69]. In another study, doping calcium phosphate cement with Mg^{2+} helped modulate macrophage inflammatory activation and suppress the expression of TNF-α and IL-6, while simultaneously upregulating the osteogenesis-related cytokine TGF-β1 [8]. However, these studies also utilized material extracts and did not account for direct cell-material interaction. In other research, Mg particles were incorporated into a poly-D,L-lactic acid matrix to enhance mesenchymal stem cell viability and osteogenic differentiation. Released Mg^{2+} ions from the composites were able to regulate the macrophage-induced inflammatory response triggered by poly-D, L-lactic acid degradation products [70,71].

Beyond the specific findings discussed above, the known biological activities of Ba^{2+} and Mg^{2+} in immune cells differ significantly and help explain the divergent effects of OCP_Sr20_Ba1 and OCP_Sr20_Mg1 observed in this study. Ba^{2+} is a well-characterized blocker of inward-rectifying K^+ channels [47], and K^+ efflux itself is a well-known trigger of NLRP3 inflammasome assembly and IL-1β maturation in macrophages, as well as a direct regulator of TNF-α and IL-8 production [72,73]. Consistent with these predominantly pro-inflammatory/cytotoxic actions, Ba^{2+} has been shown to decrease phagocyte viability, increase superoxide release, and promote apoptosis in human mononuclear phagocytes at sufficiently high concentrations [39]. In contrast, Mg^{2+} is widely known to be an anti-inflammatory and antioxidant substance in immune cells [42,43] and has been shown to directly shift THP-1-derived macrophages toward an anti-inflammatory, M2-like phenotype with reduced pro-inflammatory cytokine secretion by attenuating NF-κB activation [54]. These largely opposing direct ionic actions on macrophage ion channels, inflammasome activity, and polarization likely contribute to the divergent effects of OCP_Sr20_Ba1 and OCP_Sr20_Mg1 observed in the present study. In addition to these direct ionic effects, Ba^{2+} and Mg^{2+} ions differ significantly in ionic radius relative to Ca^{2+}, and their incorporation into the OCP crystal lattice is

known to differentially affect the crystallinity, solubility, and particle morphology of low-temperature calcium phosphates [74]. We therefore consider it likely that the different biological activities of OCP_Sr20_Ba1 and OCP_Sr20_Mg1 reflect a combination of direct ion pharmacology and ion-dependent differences in the physicochemical state of the material itself. Determining the relative contributions of these two mechanisms will require specific physicochemical characterization (e.g., ζ-potential, dissolution kinetics) of each doped composition, which we plan to conduct in future studies. It is important to highlight that these structural and morphological consequences of doping can influence cell behavior independently of the ion release itself: for calcium phosphate coatings and particles, surface topography, particle/crystallite morphology, and degree of crystallinity have been shown to directly modulate cell adhesion, proliferation, and osteogenic differentiation, with less crystalline material generally promoting lower osteogenic cell proliferation than more crystalline material of similar composition [75]. Accordingly, part of the differential response to OCP_Sr20_Ba1 compared to OCP_Sr20_Mg1 observed here may be due to such ion-induced structural differences acting directly at the cell-material interface, rather than solely to the biological activity of the released ions themselves.

Conversely, studies examining the direct interaction of micron-sized magnesium particles with macrophages observed necrosis and the secretion of pro-inflammatory cytokines [75]. Therefore, our results suggest that the observed increase in cytokine production in monocytes is most likely associated with the interaction of CP particles with cells and the subsequent alteration of intracellular processes. The differential effects of Ba^{2+} and Mg^{2+} appear to be determined not merely by their ionic composition but primarily by their influence on the structure of the calcium phosphates, which governs the nature of the material's interaction with immune cells.

It should also be noted that THP-1 cells differentiated with ATRA and PMA, although widely used as models similar to monocytes and macrophages, do not fully reproduce the phenotype and functional heterogeneity of primary circulating monocytes and tissue macrophages. Therefore, confirmation of these results in primary human cells and *in vivo* models represents an important direction for further research.

5. Conclusion

This study demonstrates the synthesis and immunomodulatory potential of low-temperature OCP co-doped with strontium and magnesium (OCP_Sr20_Mg1) or barium (OCP_Sr20_Ba1). Comprehensive physicochemical characterization confirmed the successful incorporation of dopant ions into the OCP crystal lattice, resulting in materials with altered crystallinity and structural properties.

In vitro assessment revealed a favorable biocompatibility profile: none of the materials exhibited cytotoxicity towards THP-1-derived monocyte-like (ATRA) or macrophage-like (PMA) cells. The study showed that these materials possess immunostimulatory properties. The observed effects appear to be related to the physicochemical characteristics of the synthesized materials, which determine the specifics of their phagocytosis and subsequent influence on intracellular processes, rather than being a result of the direct action of ions released into the extracellular space. Notably, the most pronounced effects were exerted on non-activated THP-1 ATRA monocyte-like cells. Among the studied materials, OCP_Sr20_Mg1 demonstrated a less significant impact on cytokine production in these cells. The observed immunomodulatory effects seem to be linked to the direct interaction of particles with the cell, influencing fundamental intracellular processes such as phagocytosis and lysosomal activity, rather than being a direct consequence of soluble ion release. The differences in biological

responses elicited by OCP_Sr20_Mg1 and OCP_Sr20_Ba1 underscore that the functional outcome is determined not only by the ionic composition but also critically depends on the resulting changes in the material's physicochemical structure.

These results confirm the promise of functional multi-ion doping as a tool for the development of modern calcium phosphate-based biomaterials with tailored immunomodulatory properties. Due to their ability to stimulate non-activated monocytes without simultaneously enhancing the activity of activated macrophages, such materials may have therapeutic potential for patients with a weakened monocytic immune response. Further research should focus on elucidating the precise intracellular signaling pathways involved in this process and confirming these effects in more complex *in vivo* bone regeneration models.

Data availability statement

No supplementary or additional data were generated in this study.

Declaration of generative AI and AI-assisted technologies

The authors did not use generative AI or AI-assisted technologies in the writing of this manuscript. The authors take full responsibility for the content of the manuscript.

Acknowledgments

This research was funded by the Russian Science Foundation, project No. 21-73-20251-П, https://rscf.ru/project/HD3xWfJ3QAuZDVJoHWq7hBoOKkOqEw-sFsFUElIhh2cSAD-EswCW6024n5D1lIUx_Xa8POIHVGg~/.

Authors' contribution

Conceptualization, V.V.M. and A.Y.T.; methodology, I.V.S. and P.V.M.; software, K.A.A.; validation, M.A.S., M.I.K. and P.V.M.; formal analysis, I.S.F. and V.S.K.; investigation, V.V.M., I.V.S., M.I.K., P.V.S., K.A.A.; resources, I.S.F., R.S.F. and V.S.K.; data curation, V.V.M.; writing—original draft preparation, V.V.M., P.V.M.; writing—review and editing, A.Y.T., I.S.F., R.S.F.; visualization, V.V.M., I.V.S., M.A.S.; supervision, V.S.K.; project administration, I.S.F. and V.S.K.; funding acquisition, A.Y.T., V.S.K. All authors have read and agreed to the published version of the manuscript.

Conflicts of interest

Vladimir S. Komlev holds the position of Associate Editor for *Biofunctional Materials* and has not peer reviewed or made any editorial decisions for this paper. The authors declare no conflicts of interest associated with this manuscript.

Abbreviations

The following abbreviations are used in this manuscript:

Areviation	Full Name
AKT1	AKT Serine/Threonine Kinase 1 (Protein Kinase B)
ATRA	All-Trans Retinoic Acid
Ba	Barium
Ba^{2+}	Barium ion
BSA	Bovine Serum Albumin
Ca	Calcium
Ca^{2+}	Calcium ion
CaP	Calcium Phosphate
CP	Calcium Phosphate
CPC	Calcium Phosphate Compound / Calcium Phosphate Cement
DCFH-DA	2',7'-Dichlorodihydrofluorescein Diacetate
DCPD	Dicalcium Phosphate Dihydrate (Brushite)
DMEM	Dulbecco's Modified Eagle Medium
ELISA	Enzyme-Linked Immunosorbent Assay
EMEM	Eagle's Minimum Essential Medium
FBS	Fetal Bovine Serum
FTIR	Fourier-Transform Infrared Spectroscopy
HAp	Hydroxyapatite
ICDD	International Centre for Diffraction Data
IL-1β	Interleukin-1 Beta
IL-6	Interleukin-6
JCPDS	Joint Committee on Powder Diffraction Standards
LPS	Lipopolysaccharide
Mg	Magnesium
Mg^{2+}	Magnesium ion
MFI	Mean Fluorescence Intensity
mTOR	mechanistic Target of Rapamycin
mTORC1	mTOR Complex 1
NALP3 (NLRP3)	NLR Family Pyrin Domain Containing 3 (Inflammasome)
NF-κB	Nuclear Factor Kappa-Light-Chain-Enhancer of Activated B Cells
OCP	Octacalcium Phosphate
PDLLA	Poly(D,L-Lactic Acid)
PI3K	Phosphoinositide 3-Kinase
PMA	Phorbol 12-Myristate 13-Acetate
RANKL	Receptor Activator of Nuclear Factor Kappa-B Ligand
ROS	Reactive Oxygen Species
rpm	Revolutions Per Minute
SEM	Scanning Electron Microscopy
SNARE	Soluble N-ethylmaleimide-sensitive factor Attachment Protein Receptor
Sr	Strontium
Sr^{2+}	Strontium ion
TGF-β1	Transforming Growth Factor Beta 1
THP-1	Human Monocytic Cell Line
TNF-α	Tumor Necrosis Factor Alpha
TRPM7	Transient Receptor Potential Cation Channel Subfamily M Member 7
XRD	X-Ray Diffraction

References

[1] Rammal H, Bour C, Dubus M, Entz L, Aubert L, *et al.* Combining calcium phosphates with polysaccharides: a bone-inspired material modulating monocyte/macrophage early inflammatory response. *Int. J. Mol. Sci*. 2018, 19(11):3458.

[2] Zhao T, Chu Z, Ma J, Ouyang L. Immunomodulation effect of biomaterials on bone formation. *J. Funct. Biomater*. 2022, 13(3):103.

[3] Lodoso-Torrecilla I, Klein Gunnewiek R, Grosfeld E, de Vries RBM, Habibović P, *et al.* Bioinorganic supplementation of calcium phosphate-based bone substitutes to improve *in vivo* performance: a systematic review and meta-analysis of animal studies. *Biomater. Sci*. 2020, 8(17):4792–4809.

[4] Jeong J, Kim JH, Shim JH, Hwang NS, Heo CY. Bioactive calcium phosphate materials and applications in bone regeneration. *Biomater. Res*. 2019, 23(1):4.

[5] Alves Côrtes J, Dornelas J, Duarte F, Messora MR, Mourão CF, *et al.* The effects of the addition of strontium on the biological response to calcium phosphate biomaterials: a systematic review. *Appl. Sci*. 2024, 14(17):7566.

[6] Teterina AY, Smirnov IV, Fadeeva IS, Fadeev RS, Smirnova PV, *et al.* Octacalcium phosphate for bone tissue engineering: synthesis, modification, and in vitro biocompatibility assessment. *Int. J. Mol. Sci*. 2021, 22:12747.

[7] Pielichowska K, Blazewicz S. Bioactive polymer/hydroxyapatite (Nano)composites for bone tissue regeneration. In *Lignin, Proteins, Bioactive Nanocomposites*. Berlin: Springer, 2010. pp. 97–207.

[8] Wang M, Yu Y, Dai K, Ma Z, Liu Y, *et al.* Improved osteogenesis and angiogenesis of magnesium-doped calcium phosphate cement via macrophage immunomodulation. *Biomater. Sci.* 2016, 4:1574–1583.

[9] Zhang M, Wan B, Sun M, Sun J, Zhu Y, *et al.* Harnessing immunomodulation: how calcium phosphate biomaterials orchestrate bone regeneration. *Tissue Eng. Part A* 2026, 32(5–6):163–184.

[10] Wan Q, Tian L, Wang M, Chen F, Li X, *et al.* Immunomodulatory effects of calcium phosphate microspheres: influences of particle size on macrophage polarization and secretion patterns. *J. Mater. Chem. B* 2025, 13(2):549–561.

[11] Hou X, Zhang L, Zhou Z, Luo X, Wang T, *et al.* Calcium phosphate-based biomaterials for bone repair. *J. Funct. Biomater.* 2022, 13(4):187.

[12] Zhang Y, Shu T, Wang S, Liu Z, Cheng Y, *et al.* The osteoinductivity of calcium phosphate-based biomaterials: a tight interaction with bone healing. *Front. Bioeng. Biotechnol*. 2022, 10:911180.

[13] Pupilli F, Ruffini A, Dapporto M, Tavoni M, Tampieri A, *et al.* Design strategies and biomimetic approaches for calcium phosphate scaffolds in bone tissue regeneration. *Biomimetics* 2022, 7:112.

[14] Li X, van Blitterswijk CA, Feng Q, Cui F, Watari F. The effect of calcium phosphate microstructure on bone-related cells *in vitro*. *Biomaterials* 2008, 29(23):3306–3316.

[15] Kaida N, Matsunaga S, Tachiki C, Otsu Y, Sugahara K, *et al.* Ridge preservation using octacalcium phosphate collagen to induce new bone containing a vascular network of mainly type H vessels. *Sci. Rep.* 2024, 14(1):25335.

[16] Sheikh Z, Abdallah MN, Hanafi AA, Misbahuddin S, Rashid H, *et al.* Mechanisms of in vivo degradation and resorption of calcium phosphate based biomaterials. *Materials* 2015, 8(11):7913–7925.

[17] Baheiraei N, Eyni H, Bakhshi B, Najafloo R, Rabiee N. Effects of strontium ions with potential antibacterial activity on *in vivo* bone regeneration. *Sci. Rep*. 2021, 11(1):8745.

[18] Birgani ZT, Gijlers S, Tahmasebi Birgani M, Yavari SA, Habibovic P, *et al.* Human mesenchymal stromal cells response to biomimetic octacalcium phosphate containing strontium. *J. Biomed. Mater. Res. A* 2016, 104(8):1946–1960.

[19] Wopenka B, Pasteris JD. A mineralogical perspective on the apatite in bone. *Mater. Sci. Eng.* C 2005, 25(2):131–143.

[20] Lomovskaya YV, Kobyakova MI, Senotov AS, Lomovsky AI, Minaychev VV, *et al.* Macrophage-like THP-1 cells derived from high-density cell culture are resistant to TRAIL-induced cell death via down-regulation of death-receptors DR4 and DR5. *Biomolecules* 2022, 12:150.

[21] Lomovskaya YV, Kobyakova MI, Senotov AS, Fadeeva IS, Lomovsky AI, *et al.* Myeloid differentiation increases resistance of leukemic cells to TRAIL-induced death by reducing the expression of DR4 and DR5 receptors. *Biochem. Mosc. Suppl. Ser. Membr. Cell Biol.* 2023, 17(1):43–57.

[22] Kobyakova M, Lomovskaya Y, Senotov A, Lomovsky A, Minaychev V, *et al.* The increase in the drug resistance of acute myeloid leukemia THP-1 cells in high-density cell culture is associated with inflammatory-like activation and anti-apoptotic Bcl-2 proteins. *Int. J. Mol. Sci*. 2022, 23(14):7881.

[23] Minaychev VV, Smirnova PV, Kobyakova MI, Teterina AY, Smirnov IV, *et al.* Low-temperature calcium phosphate ceramics can modulate monocytes and macrophages inflammatory response *in vitro*. *Biomedicines* 2024, 12(2):263.

[24] Orecchioni M. Ghosheh Y, Pramod AB, Ley K. Macrophage polarization: different gene signatures in M1 (LPS+) *vs.* classically and M2 (LPS–) *vs.* alternatively activated macrophages. *Frontiers in immunology*. 2019, 10:1084.

[25] Chen Y, Zhou L, Wang Y, Wang J, Zhang Y, *et al.* Autonomous living materials and bone-inspired scaffolds motivated by human osteogenic microenvironment mechanisms. *Mater. Des*. 2024, 244:113145.

[26] Boanini E, Gazzano M, Rubini K, Bigi A. Collapsed octacalcium phosphate stabilized by ionic substitutions. *Cryst. Growth Des.* 2010, 10(8):3612–3617

[27] Bigi A, Boanini E. Strontium-substituted calcium orthophosphates: structure, stability, morphology, and biomedical applications. *Int. J. Mol. Sci.* 2025, 26(11):5886.

[28] Bigi A, Boanini E, Capuccini C, Gazzano M. Strontium-substituted hydroxyapatite nanocrystals. *Inorganica Chimica Acta* 2007, 360(3):1009–1016.

[29] Sayahi M, Santos J, El-Feki H, Charvillat C, Bosc F, *et al.* Brushite (Ca,M) HPO_4, $2H_2O$ doping with bioactive ions (M = Mg^{2+}, Sr^{2+}, Zn^{2+}, Cu^{2+}, and Ag^{+}): a new path to functional biomaterials? *Mater. Today Chem.* 2020, 16:100230.

[30] Smirnov IV, Teterina AY, Smirnova PV, Shlykov MA, Komlev VS. Effect of Mg^{2+}, Ba^{2+}, and Sr^{2+} cation substitution on phase composition and crystal structure of octacalcium phosphate. *Inorg. Mater.* 2025, 61:475–482.

[31] Hardy D, Besnard A, Latil M, Jouvion G, Briand D, *et al.* Comparative study of injury models for studying muscle regeneration in mice. *PLoS One* 2016, 11(1):e0147198.

[32] Boanini E, Silingardi F, Gazzano M, Bigi A. Synthesis and hydrolysis of brushite (DCPD): the role of ionic substitution. *Cryst. Growth Des.* 2021, 21(3):1689–1697.
[33] You J, Zhang Y, Zhou Y. Strontium functionalized in biomaterials for bone tissue engineering: a prominent role in osteoimmunomodulation. *Front. Bioeng. Biotech.* 2022, 10:928799.
[34] Zhang W, Zhao F, Huang D, Fu X, Li X, *et al.* Strontium-substituted submicrometer bioactive glasses modulate macrophage responses for improved bone regeneration. *ACS Appl. Mater. Interfaces* 2016, 8(45):30747–30758.
[35] Liu X, Huang H, Zhang J, Sun T, Zhang W, *et al.* Recent advance of strontium functionalized in biomaterials for bone regeneration. *Bioengineering* 2023, 10(4):414.
[36] Mores L, Franca EL, Silva NA, Suchara EA, Honorio-Franca AC. Nanoparticles of barium induce apoptosis in human phagocytes. *Int. J. Nanomed.* 2015:6021–6026.
[37] Lee NH, Kang MS, Kim TH, Yoon DS, Mandakhbayar N, *et al.* Dual actions of osteoclastic-inhibition and osteogenic-stimulation through strontium-releasing bioactive nanoscale cement imply biomaterial-enabled osteoporosis therapy. *Biomaterials* 2021, 276:121025.
[38] Eslami-Kaliji F, Hedayat Nia N, Lakey JRT, Smink AM, Mohammadi M. Mechanisms of foreign body giant cell formation in response to implantable biomaterials. *Polymers* 2023, 15:1313.
[39] Nunes P, Demaurex N. The role of calcium signaling in phagocytosis. *J. Leukoc. Biol*. 2010, 88:57–68.
[40] Snipstad S, Hak S, Baghirov H, Sulheim E, Mørch Ý, *et al.* Labeling nanoparticles: dye leakage and altered cellular uptake. *Cytometry A* 2017, 91(8):760–766.
[41] Rojas-Sánchez L, Sokolova V, Riebe S, Voskuhl J, Epple M. Covalent surface functionalization of calcium phosphate nanoparticles with fluorescent dyes by copper-catalysed and by strain-promoted azide-alkyne click chemistry. *ChemNanoMat* 2019, 5(4):436–446.
[42] Baranov MV, Kumar M, Sacanna S, Thutupalli S, van den Bogaart G. Modulation of immune responses by particle size and shape. *Front Immunol*. 2021, 11:607945.
[43] Cannon GJ, Swanson JA. The macrophage capacity for phagocytosis. *J Cell Sci.* 1992, 101(4):907–913.
[44] Ten Brink T, Damanik F, Rotmans JI, Moroni L. Unraveling and harnessing the immune response at the cell-biomaterial interface for tissue engineering purposes. *Adv. Healthcare Mater*. 2024, 13(17):2301939.
[45] Saric A, Hipolito VEB, Kay JG, Canton J, Antonescu CN, *et al.* mTOR controls lysosome tubulation and antigen presentation in macrophages and dendritic cells. *Mol. Biol. Cell* 2016, 27(2):321–333.
[46] Li R, Xu J, Fu C, Zhang J, Zheng Y, *et al.* Regulation of mTORC1 by lysosomal calcium and calmodulin. *eLife* 2016, 5:e19360.
[47] Nguyen HT, Wiederkehr A, Wollheim CB, Park KS. Regulation of autophagy by perilysosomal calcium: a new player in β-cell lipotoxicity. *Exp. Mol. Med*. 2024, 56(2):273–288.
[48] Hornung V, Bauernfeind F, Halle A, Samstad EO, Kono H, *et al.* Silica crystals and aluminum salts activate the NALP3 inflammasome through phagosomal destabilization. *Nat. Immunol*. 2008, 9(8):847–856.
[49] Agidigbi TS, Kim C. Reactive oxygen species in osteoclast differentiation and possible pharmaceutical targets of ROS-mediated osteoclast diseases. *Int. J. Mol. Sci*. 2019, 20(14):3576.

[50] Tan H, Wang N, Li S, Hong M, Wang X, *et al.* The reactive oxygen species in macrophage polarization: reflecting its dual role in progression and treatment of human diseases. *Oxid. Med. Cell. Longev.* 2016, 2016(1):2795090.

[51] Ru X, Yang L, Shen G, Wang K, Xu Z, *et al.* Microelement strontium and human health: comprehensive analysis of the role in inflammation and non-communicable diseases (NCDs). *Front. Chem.* 2024, 12:1367395.

[52] Zheltova AA, Kharitonova MV, Iezhitsa IN, Spasov AA. Magnesium deficiency and oxidative stress: an update. *BioMedicine* 2016, 6(4):20.

[53] Cepeda V, Ródenas-Munar M, García S, Bouzas C, Tur JA. Unlocking the power of magnesium: a systematic review and meta-analysis regarding its role in oxidative stress and inflammation. *Antioxidants* 2025, 14(6):740.

[54] Zhou H, He Z, Cao Y, Chu L, Liang B, *et al.* An injectable magnesium-loaded hydrogel releases hydrogen to promote osteoporotic bone repair via ROS scavenging and immunomodulation. *Theranostics* 2024, 14(9):3739–3759.

[55] Jin L, Chen C, Li Y, Yuan F, Gong R, *et al.* A biodegradable Mg-based alloy inhibited the inflammatory response of thp-1 cell-derived macrophages through the TRPM7-PI3K-AKT1 signaling axis. *Front. Immunol.* 2019, 10:2798.

[56] Kim J, Gilbert JL, Lv W, Du P, Pan H. Reduction reactions dominate the interactions between Mg alloys and cells: understanding the mechanisms. *Bioact. Mater*. 2025, 45:363–387.

[57] Walz W, Shargool M, Hertz L. Barium-induced inhibition of K+ transport mechanisms in cortical astrocytes—its possible contribution to the large Ba2+-evoked extracellular K+ signal in brain. *Neuroscience* 1984, 13(3):945–949.

[58] Kovrlija I, Locs J, Loca D. Incorporation of barium ions into biomaterials: dangerous liaison or potential revolution? *Materials* 2021, 14(19):5772.

[59] Smirnov IV, Teterina AY, Fadeeva IS, Fadeev RS, Kobyakova MI, *et al.* Octacalcium phosphate doped with barium cations for application in tissue engineering. *Biophysics* 2025, 70(2):302–313.

[60] Bhoelan BS, Stevering CH, van der Boog ATJ, van der Heyden MAG. Barium toxicity and the role of the potassium inward rectifier current. *Clin. Toxicol.* 2014, 52(6):584–593.

[61] Xu J, Li Z, Zhang J, Wang Y, Wang J, *et al.* The effect of cytokines on osteoblasts and osteoclasts in bone remodeling in osteoporosis: a review. *Front. Immunol*. 2023, 14:1222129.

[62] Li W, Zhang Y, Wang Y, Li Z, Wang J, *et al.* The role of TNF-α in the fate regulation and functional reprogramming of mesenchymal stem cells in an inflammatory microenvironment. *Front. Immunol*. 2023, 14:1074863.

[63] Gerstenfeld LC, Cho TJ, Kon T, Aizawa T, Tsay A, *et al.* Impaired fracture healing in the absence of TNF-α signaling: the role of TNF-α in endochondral cartilage resorption. *J. Bone Miner. Res*. 2003, 18(9):1584–1592.

[64] Loi F, Córdova LA, Pajarinen J, Lin T, Yao Z, *et al.* Inflammation, fracture and bone repair. *Bone* 2016, 86:119–130.

[65] Yang X, Ricciardi BF, Hernandez-Soria A, Shi Y, Pleshko Camacho N, *et al.* Callus mineralization and maturation are delayed during fracture healing in interleukin-6 knockout mice. *Bone* 2007, 41(6):928–936.

[66] Majumdar S, Hira SK, Tripathi H, Kumar AS, Manna PP, *et al.* Synthesis and characterization of barium-doped bioactive glass with potential anti-inflammatory activity. *Ceram. Int.* 2021, 47(5):7143–7158.

[67] Weber K, Schilling JD. Lysosomes integrate metabolic-inflammatory cross-talk in primary macrophage inflammasome activation. *J. Biol. Chem*. 2014, 289(13):9158–9171.

[68] Sun L, Li X, Xu M, Yang F, Wang W, *et al. In vitro* immunomodulation of magnesium on monocytic cell toward anti-inflammatory macrophages. *Regen. Biomater.* 2020, 7(4):391–401.

[69] Cifuentes SC, Bensiamar F, Gallardo-Moreno AM, Osswald TA, González-Carrasco JL, *et al.* Incorporation of Mg particles into PDLLA regulates mesenchymal stem cell and macrophage responses. *J. Biomed. Mater. Res. A* 2016, 104(4):866–878.

[70] Yang F, Niu X, Gu X, Xu C, Wang W, *et al.* Biodegradable magnesium-incorporated poly(l-lactic acid) microspheres for manipulation of drug release and alleviation of inflammatory response. *ACS Appl. Mater. Interfaces* 2019, 11(26):23546–23557.

[71] Qiu MR, Campbell TJ, Breit SN. A potassium ion channel is involved in cytokine production by activated human macrophages. *Clin Exp Immunol*. 2002, 130(1):67–74.

[72] Di A, Xiong S, Ye Z, Malireddi RKS, Kometani S, *et al.* The TWIK2 potassium efflux channel in macrophages mediates NLRP3 inflammasome-induced inflammation. *Immunity* 018, 49(1):56–65.e4.

[73] Boanini E, Gazzano M, Bigi A. Ionic substitutions in calcium phosphates synthesized at low temperature. *Acta Biomater*. 2010, 6(6):1882–1894.

[74] Qadir M, Li Y, Wen C. Ion-substituted calcium phosphate coatings by physical vapor deposition magnetron sputtering for biomedical applications: a review. *Acta Biomater*. 2019, 89:14–32.

[75] Guo C, Li J, She C, Shao X, Teng B, *et al.* Bioeffects of micron-size magnesium particles on inflammatory cells and bone turnover *in vivo* and *in vitro*. *J. Biomed. Mater. Res. B Appl. Biomater.* 2016, 104(5):923–931.